

Incorporating Satellite Observations of “No Rain” in an Australian Daily Rainfall Analysis

ELIZABETH E. EBERT AND GARY T. WEYMOUTH

Bureau of Meteorology Research Centre, Melbourne, Victoria, Australia

(Manuscript received 3 November 1997, in final form 10 April 1998)

ABSTRACT

Geostationary satellite observations can be used to distinguish potential rain-bearing clouds from nonraining areas, thereby providing surrogate observations of “no rain” over large areas. The advantages of including such observations are the provision of data in regions void of conventional rain gauges or radars, as well as the improved delineation of raining from nonraining areas in gridded rainfall analyses.

This paper describes a threshold algorithm for delineating nonraining areas using the difference between the daily minimum infrared brightness temperature and the climatological minimum surface temperature. Using a fixed difference threshold of -13 K, the accuracy of “no rain” detection (defined as the percentage of no-rain diagnoses that was correct) was 98%. The average spatial coverage was 45%, capturing about half of the observed space–time frequency of no rain over Australia. By delineating cool, moderate, and warm threshold areas, the average spatial coverage was increased to 54% while maintaining the same level of accuracy.

The satellite no-rain observations were sampled to a density consistent with the existing gauge network, then added to the real-time gauge observations and analyzed using the Bureau of Meteorology’s operational three-pass Barnes objective rainfall analysis scheme. When verified against independent surface rainfall observations, the mean bias in the satellite-augmented analyses was roughly half of bias in the gauge-only analyses. The most noticeable impact of the additional satellite observations was a 66% reduction in the size of the data-void regions.

1. Introduction

Estimates of the spatial distribution of rainfall on short timescales (daily or less) are important for many real-time applications such as agricultural water management, drought monitoring, flood forecasting, and dynamic initialization and verification of numerical weather prediction models. These applications require that the rainfall estimates be both accurate and timely with adequate coverage over the region of interest.

The Australian Bureau of Meteorology produces an operational daily rainfall analysis covering the land area of Australia at a spatial resolution of 0.25° latitude and longitude (Weymouth et al. 1998). An example of the daily rainfall analysis is shown in Fig. 1 for 24 December 1996. Large regions labeled as “no data” are seen in central Australia. Climatological rainfall measurements show that the interior of Australia is normally very dry (Drosowsky 1993). It is likely that most of the data-void regions in this analysis actually experienced no rain, but without gauge observations it is difficult to be certain. This situation is typical of near-real

time rainfall analyses in Australia. It would be desirable to fill in these data-void regions using observations from other sources, if possible.

This paper develops and tests a method for using geostationary infrared (IR) satellite data to define regions of no rainfall, with the goal of producing a more complete and accurate daily rainfall analysis. A simple threshold technique detects warm regions, signifying the absence of potential rain-bearing clouds, and assigns pseudo-observations of “no rain” to these regions. In addition to providing some information in the gauge-void regions, the insertion of satellite observations better defines the boundaries between raining and dry regions in areas with sparse gauge coverage. The satellite observations are inserted into the objective rainfall analysis and their impact is measured for 238 days during October 1996–August 1997. Verification of the augmented analyses against independent rainfall observations demonstrates the utility of this technique. Finally, ideas for improving the rainfall analysis are discussed.

2. Rainfall measurements in Australia

Figure 2 shows the location of the approximately 6000 rain gauges measuring rainfall over Australia. Of these, approximately 400 are located at synoptic stations that report reliably every day, about 1500 are telegraphic

Corresponding author address: Dr. Elizabeth Ebert, Bureau of Meteorology Research Centre, GPO Box 1289 K, Melbourne, Victoria 3001, Australia.
E-mail: e.ebert@bom.gov.au

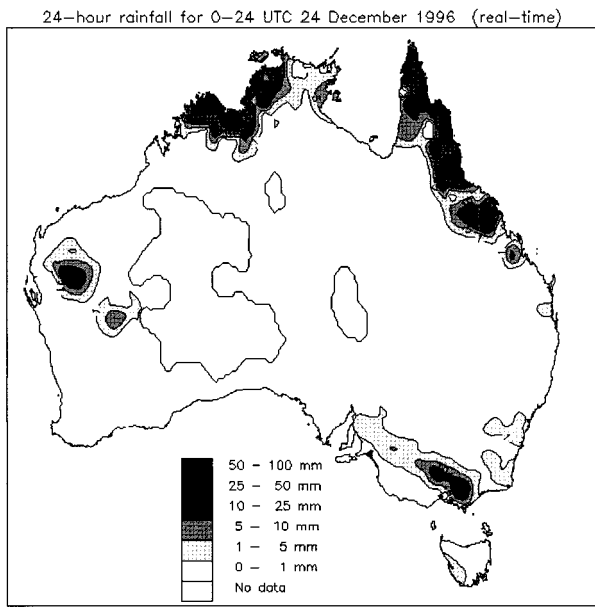


FIG. 1. Analysis of real-time rain gauge data for 24 December 1996.

stations that do not report every day, and the remainder are cooperative network sites that send a report of daily rainfall to the Bureau of Meteorology at the end of each month. Although the number of gauges is large, their distribution is very uneven. Over most of the coastal regions of southeastern and southwestern Australia the spatial coverage of gauges is quite dense, while the remainder of the country has only sparse coverage. In fact, in large desert regions in Western Australia, the Northern Territory, and South Australia there are no surface rainfall observations at all. We note that this situation is by no means unique to Australia.

The sparsity of the data in some regions is compounded by two reporting practices that make some information unusable. First, the telegraphic stations report daily rainfall only when there is measurable precipitation. "No report" from a telegraphic site is likely to mean that no rain fell, but it could also result from personnel or communications errors. To forestall this danger, no report from a telegraphic station is treated as no data. Second, many telegraphic stations report daily rainfall from Tuesday to Friday, with the Monday report corresponding to a 3-day rainfall total. This means that there are many fewer observations of daily rainfall on Saturdays, Sundays, and Mondays than on the other days of the week.

Radar observations are used operationally to detect

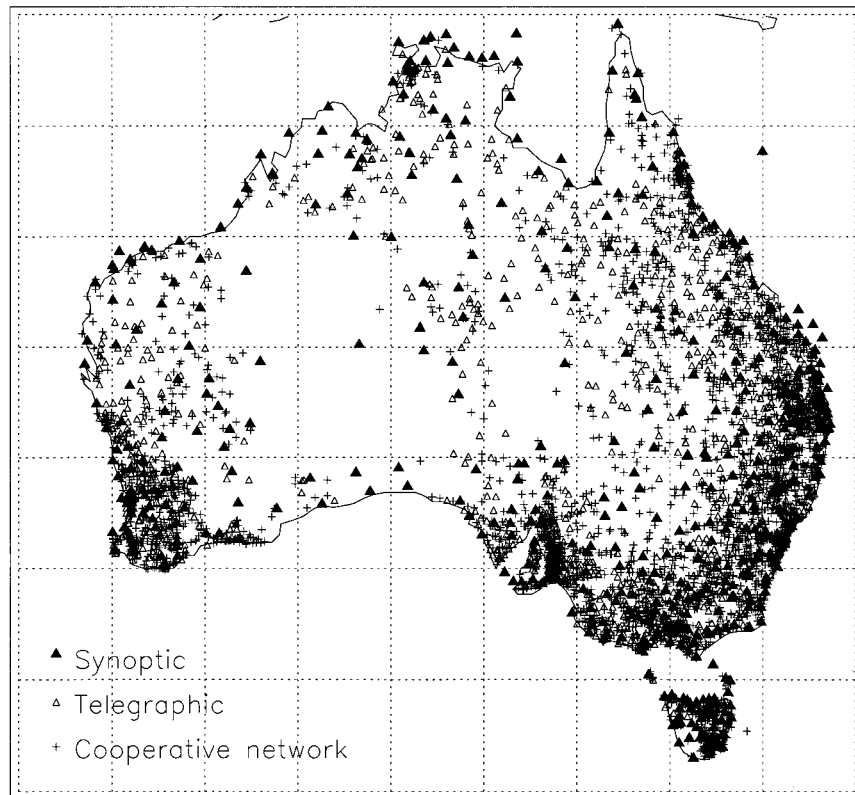


FIG. 2. Australian surface rainfall observations network.

TABLE 1. Typical characteristic of rain systems (after Sumner 1988).

Type	Depth	Temperature	Extent	Lifetime	Rain rate
Convective	Moderate to deep	>40° colder than surface	1–50 km	30 min to several hours	Intense bursts
Frontal system	Variable	>30° colder than surface	Broad, often elongated	Days	Light to heavy
Shallow convection (stream weather)	Shallow	>10° colder than surface	10s to 100s of km	Minutes to hours	Drizzle, light rain
Orographic	Shallow	>10° colder than surface	Usually narrow	Hours	Light to moderate

areas of precipitation at high temporal and spatial resolution (typically about 10 min and a few square kilometers). The Bureau of Meteorology operates 40 weather radars located mainly along the populated coastal zones. With the exception of the polarimetric radar site in Darwin (Keenan and Manton 1996), these radars have not been carefully calibrated to yield accurate estimates of rain rate. Rough estimates may be made within about a 100-km radius of the radars using a standard Z – R reflectivity–rain rate relationship. Simple indications of rain–no rain may be obtained out to a distance of a few hundred kilometers from the radars. Further discussion and utilization of radar data is beyond the scope of this study, except to note that we intend to incorporate this useful source of rainfall information in future rainfall analyses.

Another data source is satellite imagery from the Japanese Geostationary Meteorological Satellite (GMS). Infrared satellite imagery from geostationary satellites has been used to determine estimates of rainfall from space for nearly 30 years. Barrett (1970) and Arkin (1979) were among the first to quantify the relationship between the fractional coverage (or frequency) of cold cloud-top temperatures and the amount of rainfall measured at the surface in the Tropics. A simple IR threshold algorithm emerged, called the Geostationary Operational Environmental Satellite (GOES) Precipitation Index (Arkin and Meisner 1987), which is currently used by the Global Precipitation Climatology Project to estimate monthly rainfall equatorward of 40° latitude.

Infrared algorithms have also been employed to estimate rainfall on daily and shorter timescales. A review of their performance indicates that the ability of IR algorithms to correctly estimate daily rainfall is dependent on the regime in question (Ebert et al. 1996). Ebert and Le Marshall (1995) tested three IR algorithms over Australia and found that they detected the occurrence of rain in a 24-h period with an average accuracy of 64%. All of the techniques overestimated the rainfall amount, with rms errors several times greater than the mean observed rain rate. These algorithms suffered from two opposing errors: the incorrect detection of rainfall in cold, nonprecipitating cirrus clouds, and the failure to detect rain in (relatively) warm stratiform clouds, particularly in southern regions. Experience with these satellite algorithms suggests that the basic premise of rainfall being associated primarily with cold cloud-top temperatures often does not hold true outside tropical

regions. We conclude that IR rainfall estimates are simply not accurate or reliable enough to provide quantitative daily rainfall amounts to supplement the gauge observations in Australia.

However, we may be able to use IR observations from geostationary satellites to indicate where it *has not rained*. If potential rain clouds can be accurately detected, then the absence of any such clouds can be treated as an observation of no rain. Satellite imagery is used in this fashion to manually check for erroneous rain detection in radar observations due to anomalous propagation (e.g., UKMO/NRA 1992). This approach is analogous in many ways to the cloud-clearing algorithms used in other surface remote sensing applications (e.g., Saunders and Kriebel 1988).

3. Satellite no-rain algorithm

a. Methodology

Table 1 lists some attributes of different types of rain clouds. Most rain clouds have temperatures that are easily distinguishable from surface temperatures, as well as lifetimes and horizontal extents that are great enough to be observed by geostationary satellites. GMS observations are made at hourly intervals, supplemented by four additional half-hourly observations for wind derivation. The spatial resolution of GMS pixels is about 5 km. This frequency and resolution should be sufficient to capture most rain-bearing clouds.

The simplest method for detecting potential rain clouds from satellite IR measurements involves setting a threshold brightness temperature. Observations that are colder than this threshold are called “cloudy,” while observations that are warmer are called “clear.” The threshold temperature of 253 K (–20°C) is a commonly used value for isolating potential rain clouds (e.g., Negri et al. 1984; Adler and Negri 1988; Goodman et al. 1993). The choice of a threshold temperature is problematic. A threshold that is too warm will be too restrictive, and many clear regions will be mislabeled as cloudy. A threshold that is too cool will detect most of the clear regions but may allow some cloudy, possibly rainy, observations to be misclassified as clear. The optimum threshold should strike a balance between “playing it safe” and being too “permissive.”

Because Australia comprises many climatic regimes, the use of a fixed threshold temperature is inappropriate.

A threshold that is appropriate for the tropical north will certainly not yield optimum cloud discrimination in the cooler south, and thresholds that work well in summer may not work well in winter. Some cloud detection algorithms use dynamic threshold allocation, whereby a region is searched for warm (surface) pixels, and the threshold is set at some increment below the derived surface temperature (Coakley 1988). Albedo thresholds in accompanying visible imagery can also be included in this approach. While intuitively attractive, this method is computationally intensive and relies on the presence and accurate identification of surface pixels in the search area.

It may be that a simpler method can provide the information we need. At the very least, a rain cloud threshold should be a function of location and time of year. This approach was taken by Todd et al. (1995) in their investigation of satellite differentiation of rain–no-rain areas in the Nile River Basin. In this study we investigate the use of a rain cloud detection threshold temperature based on the expected minimum surface temperature. These were obtained from the Bureau’s National Climate Centre as analyses of monthly mean minimum surface temperature on a 0.25° latitude–longitude grid. It would be possible, in principle, to use gridded observed daily minimum surface temperatures, but these are not yet operationally available, and moreover, we will show that very good results are achievable using the climatological estimates.

For 238 days during the period 22 October 1996–25 August 1997 the daily surface rainfall observations from the real-time gauge network were collected. Also collected were daily minimum GMS brightness temperature composites, $(T_{\min})_{\text{GMS}}$, for the same period. These were derived by selecting the coldest temperature observed at each pixel location over the 24-h period. If more than 20% of GMS images were missing from a 24-h period, that day’s data were discarded. The GMS minimum temperature composites were averaged onto the same 0.25° grid used by the minimum surface temperature fields, $(T_{\min})_{\text{clim}}$ and the bureau’s operational daily rainfall analysis. The $(T_{\min})_{\text{clim}}$ fields were interpolated in time to the dates of the GMS images, then subtracted from the GMS composites to derive fields of minimum temperature difference, $\Delta T_{\min} = (T_{\min})_{\text{GMS}} - (T_{\min})_{\text{clim}}$. Note that ΔT_{\min} is largely independent of the broad seasonal and regional variations found in the raw temperature fields. As such, it may be possible to choose a threshold value, ΔT_{\min}^* , that is appropriate for all regions and seasons.

To determine an appropriate threshold, it is necessary to examine the joint distribution of ΔT_{\min} and rainfall observations. The difference fields ΔT_{\min} were interpolated to the locations of the rain gauges to obtain a matched set of over 270 000 observations. Of these, approximately half (133 528) were made at synoptic stations that report every day. The remaining observations were at telegraphic stations and represent mainly

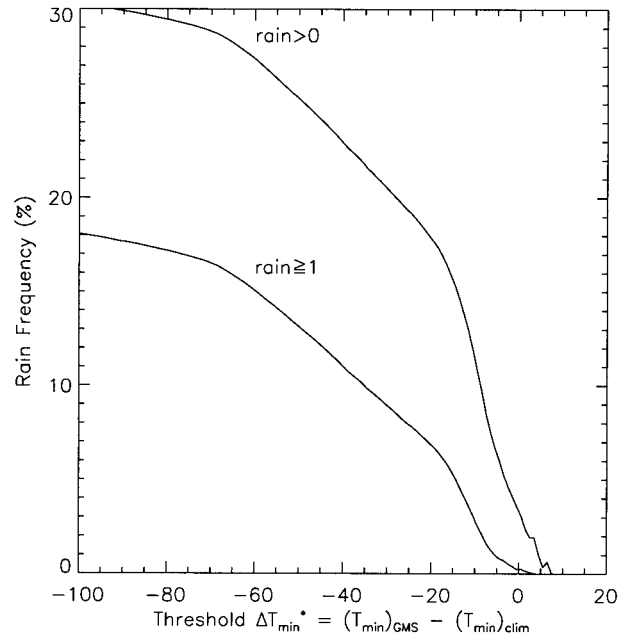


FIG. 3. Frequency of rain for all observations of $\Delta T_{\min} \geq \Delta T_{\min}^*$ for rain thresholds of 0 and 1 mm day⁻¹.

those occasions when measurable rainfall was observed. The set of synoptic observations thus gives a better indication of rainfall frequency than does the complete set of observations, although both are biased toward the greater density of stations in southwestern and southeastern Australia.

From the matched set of N observations of $(\Delta T_{\min}, \text{rainfall})$ at synoptic stations we compute, for each potential threshold value, ΔT_{\min}^* , the frequency of ΔT_{\min} measurements at or above the threshold, for which rainfall was observed:

$$f(\text{rain} | \Delta T_{\min} \geq \Delta T_{\min}^*) = \frac{N_{\text{rain}, \Delta T_{\min} \geq \Delta T_{\min}^*}}{N_{\Delta T_{\min} \geq \Delta T_{\min}^*}} \quad (1)$$

This gives an estimate of the probability that a satellite estimate of no rain, based on a threshold of ΔT_{\min}^* , is erroneous. Figure 3 shows the percentage of observations exceeding each ΔT_{\min}^* for which rainfall was observed. Eighty-two percent of observations with $\Delta T_{\min} \geq -20$ K correspond to zero rainfall, and 93% of observations with $\Delta T_{\min} \geq -20$ K correspond to rain less than 1 mm day⁻¹. Ninety-seven percent of observations with $\Delta T_{\min} \geq -10$ K correspond to rain less than 1 mm day⁻¹ (note that 1 mm day⁻¹ is the minimum rainfall contour commonly used on daily rainfall analysis charts). This means that ΔT_{\min} can be a very reliable indicator of no rain, depending on the threshold value chosen.

The overall error rate for all observations is given as a function of threshold ΔT_{\min}^* in Fig. 4. This is the frequency of error that would occur if all observations for which $\Delta T_{\min} \geq \Delta T_{\min}^*$ were to be labeled as no rain:

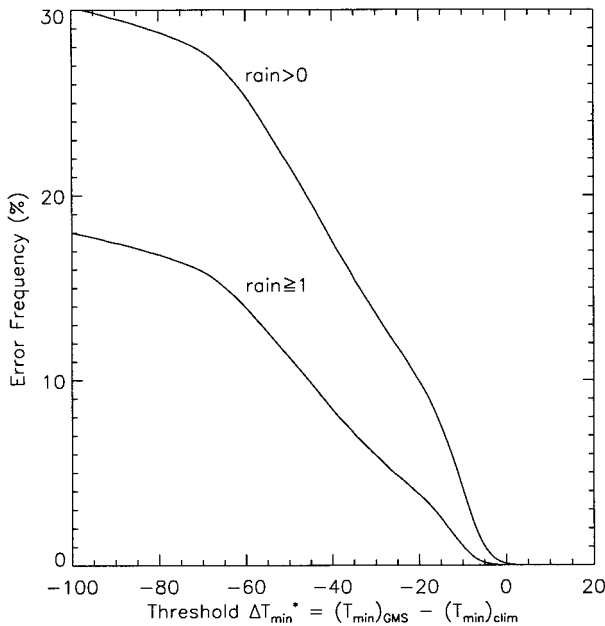


FIG. 4. Frequency of overall error in satellite no-rain determination as a function of threshold, ΔT_{min}^* for rain thresholds of 0 and 1 mm day⁻¹.

$$f(\text{rain}) = \frac{N_{\text{rain}, \Delta T_{min} \geq \Delta T_{min}^*}}{N} \quad (2)$$

Note that since we are primarily concerned with minimizing the occurrence of the satellite algorithm's estimating zero rainfall when rain was actually observed, we do not consider satellite diagnoses of "possible rain" in zero-rainfall situations to be erroneous. For nonzero rain GMS observations of ΔT_{min} could be used to detect no-rain areas with 95% accuracy using a threshold of $\Delta T_{min}^* = -11$ K. To achieve 99% accuracy, a threshold of -5 K is required. When the definition of "rain" is increased to 1 mm day⁻¹ or greater, then the threshold can be significantly lowered. Ninety-five percent accuracy can be achieved using a threshold of $\Delta T_{min}^* = -25$ K, and 99% accuracy occurs for $\Delta T_{min}^* = -10$ K.

b. Discussion of errors

Errors in no-rain detection occur because some rain clouds are not being detected in the GMS minimum brightness temperature imagery. Figure 5 shows the frequency of incorrect diagnoses of no rain over Australia for thresholds ΔT_{min}^* of -25 , -13 , and -10 K, corresponding to accuracies of 95%, 98%, and 99%, respectively. A plot of the Australian topography is shown in Figure 6. Most of the errors in no-rain detection occur

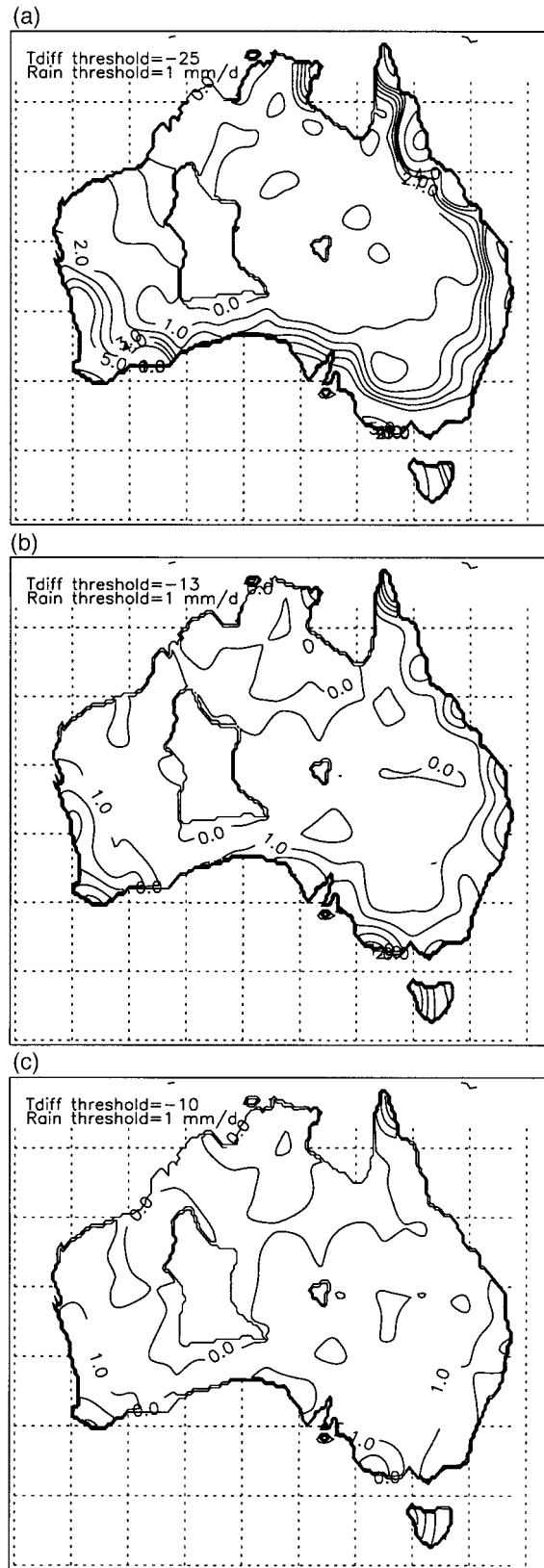


FIG. 5. Distribution of error frequency (%) in the satellite determination of no rain using thresholds of (a) -25 , (b) -13 , and (c)

-10 K. Contour intervals are 0, 1, 2, 3, 4, 5, 10. The "hole" in west-central Australia corresponds to a region with no gauges.

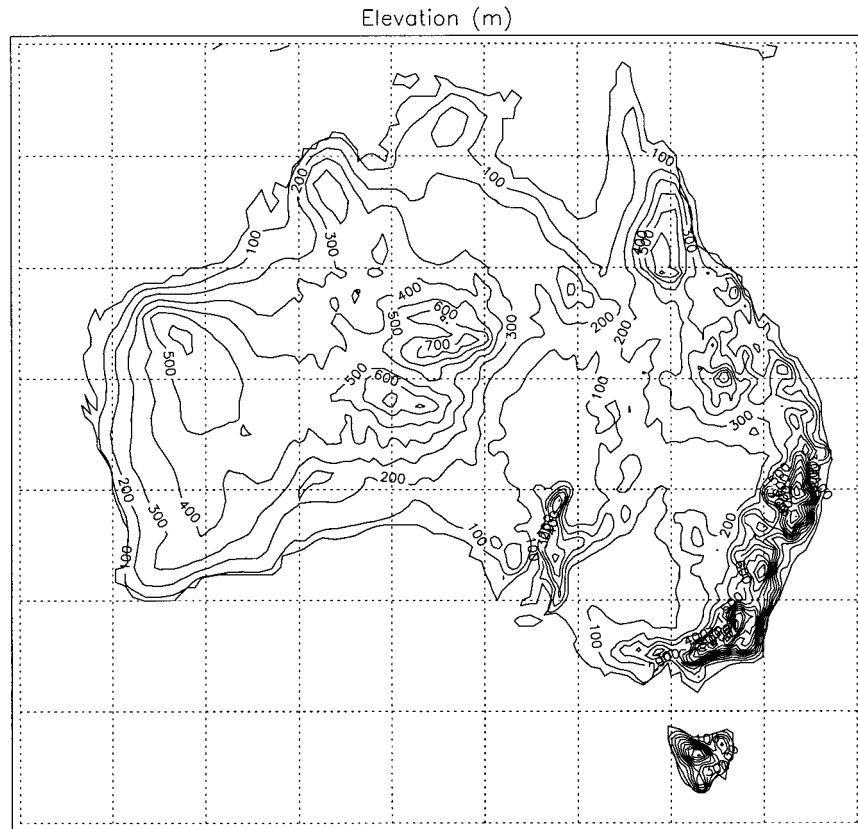


FIG. 6. Topography of Australia. The contour interval is 100 m.

in the mountainous and coastal regions. These are regions where orographic lifting and moisture convergence can produce showers in shallow low-level clouds that may not be very much cooler than the surface (see Table 1). The clouds themselves may be narrow or broken, only partially filling the 5-km GMS satellite field of view, compounding the difficulty in their detection. As the threshold is raised to warmer temperatures, the frequency of error is reduced but not eliminated in these regions. This suggests the possibility of using multiple thresholds for regions with different degrees of risk—this approach will be demonstrated later.

Another potential cause of error is the occasional absence of GMS hourly imagery due to eclipses or ingest failures. If a gap of 2 or more hours occurs in the 24-h minimum temperature composite, precipitating clouds may either develop in or advect through a region in the elapsed time between observations. Such gaps occurred on 40% of the days examined. A comparison of the average error for days with full and incomplete coverage revealed that the error rate for days with gaps was 22% higher, in relative terms, than for days with complete temporal coverage.

Another explanation for some rainfall observations apparently occurring with warm IR temperatures is a slight mismatch between the timing of the satellite and

surface rainfall observations. The GMS minimum temperature data is derived from imagery beginning at 0030 and ending at 2330 UTC, whereas the rain gauges are checked at roughly 0900 LT. This can vary between 2200 and 0100 UTC, depending on the location and time of year. If rain begins or ends in the few hours where the dates may be mismatched, it will be incorrectly associated with the wrong day's temperature.

c. Spatial coverage

Presuming that a small error in rain detection is considered acceptable in exchange for a greater number of surrogate no-rain observations from satellite, how much additional spatial coverage would be gained? Figure 7 shows the average percentage of the area in Australia that would be diagnosed as no rain for each threshold, ΔT_{\min}^* , plotted as a function of the average accuracy achieved using that threshold. In Fig. 7a rain is defined as any measurement greater than 0 mm day^{-1} , while the lower plot considers no rain to be any measurement less than 1 mm day^{-1} . In the conservative case of a maximum allowable error of 1% in the detection of zero rainfall ($\Delta T_{\min}^* = -5 \text{ K}$, from Fig. 4), the average coverage would be about 17%, as shown in Fig. 7a. However, if 5% error in the determination of areas with rain

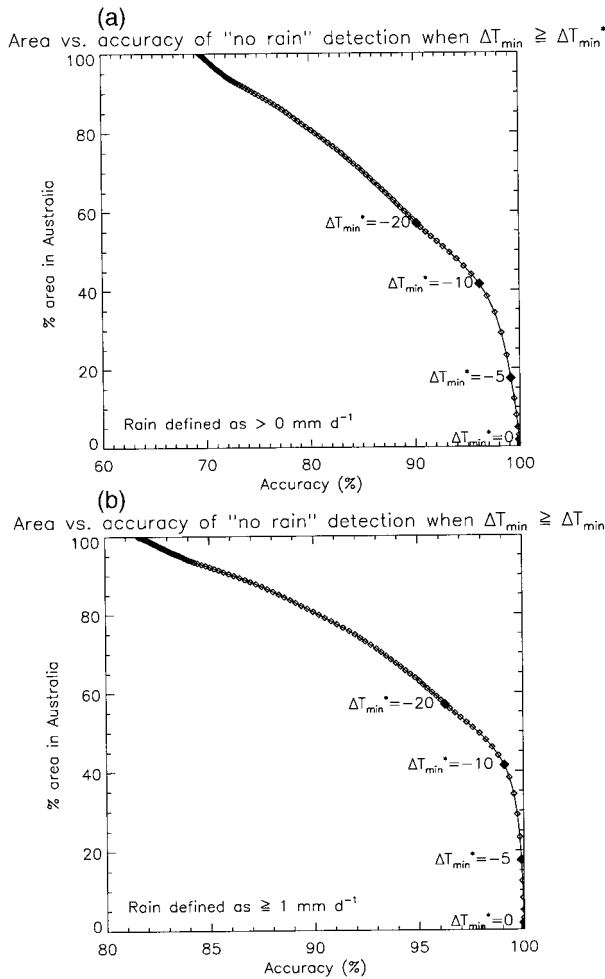


FIG. 7. Average percentage area of Australia that would be diagnosed as no rain for each threshold, ΔT_{\min}^* , plotted as a function of the average accuracy achieved using that threshold, for rain defined as (a) greater than 0 mm day^{-1} and (b) greater than or equal to 1 mm day^{-1} .

less than 1 mm day^{-1} was considered acceptable, then a threshold of around -25 K could be set, and the area satisfying this criterion would average over 60% of Australia. Even a more moderate allowable error of 2% for rain less than 1 mm day^{-1} ($\Delta T_{\min}^* = -13 \text{ K}$) would, on average, yield surrogate no-rain observations over about 45% of Australia. The space-time average frequency of no-rain observations determined from gauges for the period under consideration is 88%. The satellite observations thus capture approximately half of the actual no-rain frequency.

d. Increased reliability using multiple thresholds

In Fig. 5 it was seen that the greatest frequency of errors occurred along the coastal regions in areas of pronounced topography. Conceptually, these coastal and topographic regions can be viewed as "high risk"

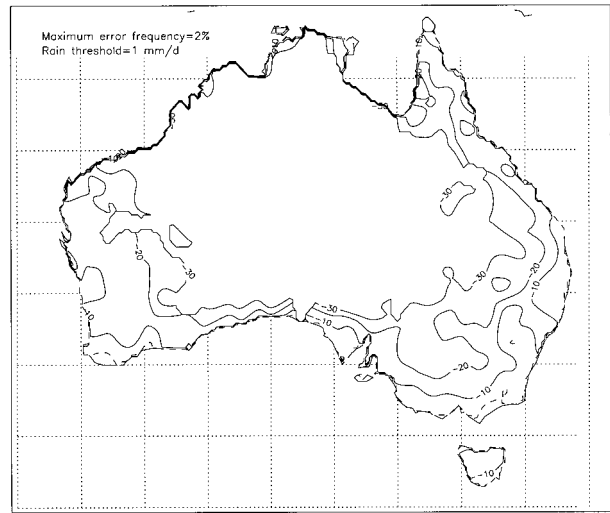


FIG. 8. Temperature difference threshold, ΔT_{\min}^* , for which the error frequency does not exceed 2%.

regions, in that the use of the -25 K threshold produces significantly greater than average error frequencies there. Analogously, the interior portions of the continent can be considered as "low risk" regions. One way to achieve high accuracy over the entire continent without sacrificing very much spatial coverage would be to use multiple thresholds, that is, a cool threshold for the low-risk areas and a more conservative, warmer threshold for the high-risk areas.

Using the matched (ΔT_{\min} , rainfall) observations, the threshold at each station for which the error frequency equaled 2% or less was determined. These threshold values, ΔT_{\min}^* , were then analysed onto a 0.25° grid (Fig. 8). Throughout most of the interior of Australia, ΔT_{\min}^* is colder than -30 K . The warmest values, between -10 and -5 K , are found in the coastal regions of southwestern and southeastern Australia, and in the northernmost tropical regions. In the data-void regions of western and central Australia we do not know the value of ΔT_{\min}^* because there are no stations, but we may reasonably expect it to be a cold value in keeping with the other regions in the interior of Australia.

From Fig. 8, categories for cool, moderate, and warm thresholds, and unacceptable risk are defined as follows:

$$\text{Cool threshold (low risk)} \quad \Delta T_{\min}^* \leq -30 \text{ K},$$

$$\text{Moderate threshold (moderate risk)} \quad -30 \text{ K} < \Delta T_{\min}^* \leq -20 \text{ K},$$

$$\text{Warm threshold (high risk)} \quad -20 \text{ K} < \Delta T_{\min}^* \leq -10 \text{ K},$$

and

$$\text{Unacceptable risk} \quad \Delta T_{\min}^* > -10 \text{ K}$$

Within each of these groups the threshold value used for determining the satellite no-rain estimates is conservatively chosen, that is, $\Delta T_{\min}^* = -30 \text{ K}$ for the low-

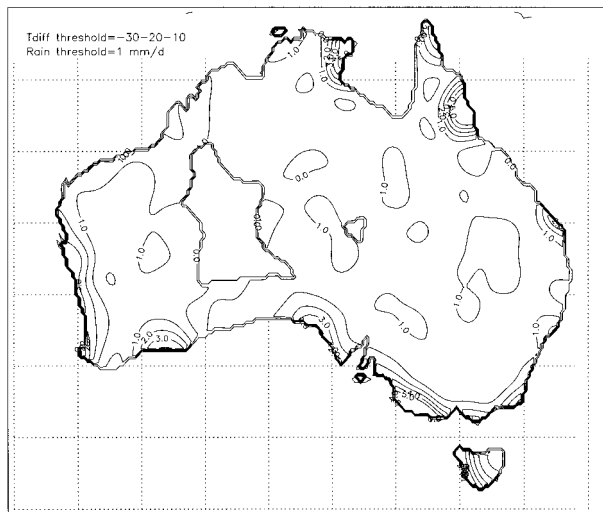


FIG. 9. Distribution of error frequency (%) in the satellite determination of no rain using multiple thresholds of -30 , -20 , and -10 K for low-, moderate-, and high-risk areas, respectively.

risk area, -20 K for the moderate-risk area, and -10 K for the high-risk area. No satellite no-rain estimates are produced inside the regions classified as an unacceptable risk.

Figure 9 shows the distribution of error frequency when the multiple thresholds were applied to the daily minimum temperature difference imagery. The average accuracy at synoptic stations was 98.2% (the spatially averaged accuracy was slightly higher, 99.1%). Small regions with error frequency exceeding 2% occurred because the analysis procedure smooths the ΔT_{\min}^* values determined using the station data. Fortunately, these areas also have sufficient gauge coverage, so errors in satellite no rain determination will have little impact on the final rainfall analysis there. The average spatial coverage achieved using multiple thresholds was 54% over the whole of Australia and 66% in the data-void regions. This is significantly greater than the 45% coverage achieved using a single threshold of -13 K (Fig. 7b).

The procedure was repeated using an error criterion of 5% instead of 2% with the threshold categories defined as before. This experiment resulted in a station average accuracy of 97.1%, and an average spatial coverage of 63% over Australia and 66% in the data-void regions. Although the average spatial coverage over Australia was greater for the latter trial, there was no difference in spatial coverage over the data-void regions. In view of the greater accuracy of the first trial, it was decided to adopt the more restrictive threshold categories based on the contours of ΔT_{\min}^* for the 2% error criterion. Although a 2% error criterion may seem rather arbitrary, we consider that accepting this level of error in exchange for 54% average spatial coverage is a reasonable compromise between playing it safe and achieving maximum coverage with the satellite observations.

4. Improvement of rainfall analyses with satellite no-rain estimates

a. Daily rainfall analysis

The Bureau of Meteorology's real-time operational daily rainfall analysis produces a 0.25° gridded field of rainfall a few hours following the 0900 LT reporting time, using up to 1900 observations from synoptic and telegraphic stations (Fig. 2). However, because of the usual practice of the telegraphic stations to report only when there is measurable rainfall, the total number of stations reporting on a daily basis is usually more like 500–1000.

The objective analysis scheme is a three-pass Barnes successive corrections method (Achtemeier 1987). This procedure uses distance weighting to determine grid-point values of rainfall from the irregularly spaced observations. The weights are given by a Gaussian function of distance from the station, with a "length scale" describing the distance at which the weight equals 0.5. Starting with a background field of zero, the first pass uses a length scale of 80 km (determined from the average station spacing) and produces a relatively smooth rainfall field. The second and third passes employ a smaller length scale of 44 km and add greater detail to the rainfall analysis. Grid points with summed first-pass station weights of less than 0.2 are considered unreliable and are termed "data void." The daily rainfall analyses regularly contain large data-void regions in central Australia. Further details of the operational daily rainfall analysis are given by Weymouth et al. (1998).

A prime objective in detecting nonraining areas from satellite data is to use this information to produce a more accurate rainfall analysis. The satellite observations have the potential to improve the analyses in three ways. Most importantly, they provide some information in the data-void regions, yielding a more spatially complete analysis than is possible without the addition of satellite observations. Second, in data sparse areas the insertion of satellite observations can better define the boundaries between raining and dry regions. And third, satellite no-rain observations can be used in the quality control process for the station observations. For example, an isolated report of a very large rainfall amount may be flagged as suspicious if it is surrounded by many satellite observations of no rain.

b. Insertion of GMS no-rain estimates

The most logical way to include the satellite no-rain observations is to treat them as additional input to the objective analysis scheme. Adding the satellite no-rain observations before performing the objective analysis is likely to reduce some of the overestimation of rain area and amount that occurs when rain from sparsely spaced gauges is "smeared" by the analysis into surrounding regions that may not have experienced rain. Weymouth et al. (1998) chose a moderate length scale

of 80 km to use in the real-time analysis in order to yield reasonably reliable estimates of rainfall without creating too many gaps in the analysis. They showed that in regions where convective precipitation is the predominant type, the use of the 80-km length scale produced real-time analyses that gave 10%–20% more rain, on average, than did the more accurate analysis made later when observations from the cooperative network were included. They suggested that a smaller length scale was more appropriate for convective regions.

When adding the satellite no-rain observations to the existing gauge observations, it is important not to swamp the existing gauge network with satellite data, which would reduce the relative importance of actual rainfall observations. The satellite observations must be sampled to a density compatible with the existing gauge observations where possible. The sampling strategy we adopt is to replace the no-report status from telegraphic stations with satellite estimates of zero rainfall whenever ΔT_{\min} exceeds ΔT_{\min}^* . Support for this strategy comes from an experiment described by Weymouth et al. (1998) in which the received real-time rain observations were augmented with reports of no rain from telegraphic stations (received at the end of the month). The analyses produced using the augmented data showed only small differences from the analyses produced using the full 6000-station climatological dataset. This suggests that the majority of the bias in the real-time analyses could be eliminated if reports of no rain at the locations of telegraphic stations were available. In the data-void regions we insert satellite estimates of zero rainfall at a density of one observation per $(75 \text{ km})^2$.

In principle, the satellite observations could be assigned weights that would depend on the amount of assumed error inherent in the choice of a particular threshold ΔT_{\min}^* , and also on the completeness of the daily minimum temperature composite (i.e., the number of IR images in the 24-h period). For now we give the satellite observations equal weight with the gauge observations. The data are then analysed using the Barnes objective analysis scheme described above.

c. Example of 25 December 1996

Figure 1 showed an example of the operational real-time rainfall analysis using gauge data alone for rain occurring between 0000 and 2400 UTC on 24 December 1996. On this day there were regions of convective rainfall across northern and northeastern Australia and frontal precipitation in the southeast. The data-void regions in western and central Australia are clearly seen.

The corresponding ΔT_{\min} image is shown in Fig. 10. The darker shades correspond to warmer values of ΔT_{\min} . The surface observations have been superimposed on the image with “○” indicating no rain, “+” indicating rain less than 1 mm day^{-1} , and “*” indicating rain of at least 1 mm day^{-1} . Note that the rain areas correspond well to areas of cold temperatures (large

negative ΔT_{\min}) except along the northeast coast where the rain appears to have been associated with fairly shallow cloudiness.

The no-rain algorithm with multiple thresholds was applied to the ΔT_{\min} image to produce a binary image of no rain and “possible rain.” This was sampled to the locations of the nonreporting telegraphic stations, and to 75-km spatial resolution in the data-void regions, as described above. The location of the satellite no-rain observations is shown in Fig. 11 along with the rain gauge observations from synoptic and (reporting) telegraphic stations. A large number of satellite observations have been added. The original number of real-time station reports was 723; excluding satellite observations over the oceans, the satellite observations added 616 further estimates of no rain at the locations of nonreporting telegraphic stations and 79 estimates in the data-void regions, nearly doubling the total number of observations. The majority of the diagnosed no-rain sites lie far from the observations of measurable precipitation. Only along a small stretch of the northeast coast are satellite no-rain estimates found in close proximity to rain observations.

The analysis of gauge and satellite observations is shown in Fig. 12. Compared to the gauge-only analysis (Fig. 1) the size of the data-void regions has been reduced dramatically. The rain areas in the augmented analysis are similar to those in the gauge-only analysis, with the main difference being a lighter rainfall pattern along the northeast coast in the augmented analysis. An analysis prepared using all available surface observations (synoptic, telegraphic, and cooperative network) is shown in Fig. 13. The addition of observations from the cooperative network adds detail to the rainfall analysis, increasing the rainfall area in central northern Australia and reducing it in other regions. When checked against this more accurate analysis, the satellite-augmented analysis presented a far truer picture of the actual rain along the northeast coast than did the real-time analysis without satellite data (the pattern correlation of the satellite-augmented analysis with the analysis using all surface observations was 0.86, while the corresponding value for the real-time analysis was 0.82).

d. Verification of rainfall analyses

To determine the impact of including the satellite pseudo-observations of no rain on analysis errors, the real-time gauge observations were analyzed with and without the addition of satellite observations and verified against independent daily rainfall observations from the cooperative network for the period from 22 October 1996 to 22 May 1997. Table 2 compares the resulting verification statistics.

The augmented analyses had substantially smaller bias than did the gauge-only analyses. As the statistics for the dry stations show, the bias reduction is due in part to reduced “smearing” of rainy areas in the analysis

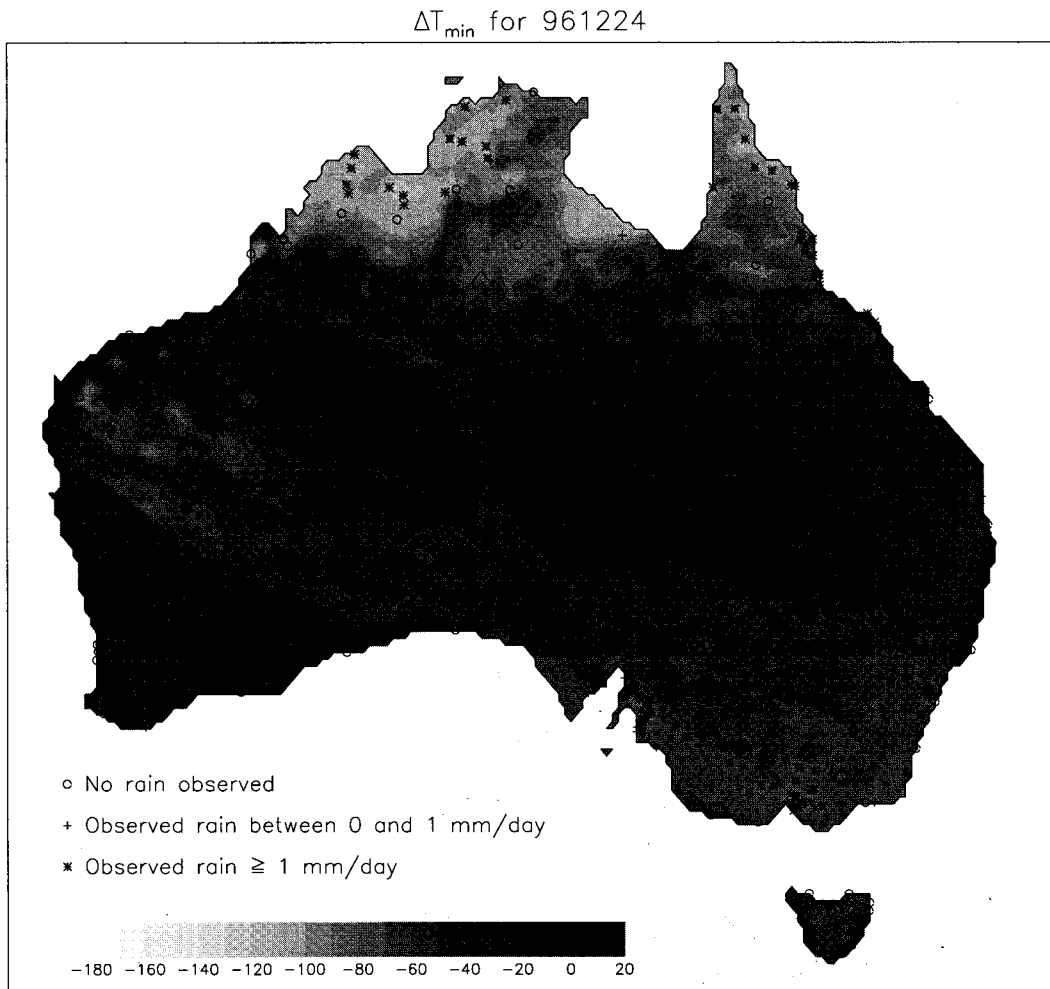


FIG. 10. Field of ΔT_{\min} corresponding to GMS imagery for 24 December 1996. The darker shades correspond to warmer values of ΔT_{\min} . The surface rainfall observations R are superimposed (○: $R = 0$ mm day⁻¹, +: $0 < R < 1$ mm day⁻¹, *: $R \geq 1$ mm day⁻¹).

when satellite no-rain observations replaced missing reports from telegraphic stations. Missed rainfall events in the satellite observations also had an effect on the bias, as indicated by the verification statistics for raining stations. The reduction in bias occurs almost entirely in the northern (warmer) half of Australia. Figure 14 shows the bias fields computed as the average difference between the real-time and National Climate Centre daily rainfall analyses (using all available surface observations) for the gauge-only and satellite-augmented cases. The addition of satellite no-rain observations reduces, but does not eliminate, the overestimation of rainfall in convective regimes. The lesser influence of satellite data in the south is due both to the abundance of rain gauges in that part of the country and the more widespread nature of rain events.

The rms and mean absolute errors for the augmented analyses were not significantly different from those for the gauge-only analyses. This indicates that the addition

of satellite no-rain observations did not have a detrimental effect on the final rainfall analysis. Indeed, the provision of some data in the data-void regions, along with a dramatic reduction in overall bias, leads to the conclusion that the addition of satellite no-rain observations has a very beneficial impact on the rainfall analysis.

5. Summary and conclusions

We have shown that geostationary satellite observations can be used to distinguish potential rain-bearing clouds from nonraining areas, providing reliable surrogate observations of no rain over large areas. The use of ΔT_{\min} , defined as the difference between the satellite observed minimum brightness temperature and climatological minimum surface temperature, to define the no-rain threshold accounted for much of the seasonal and regional dependence that would be expected using

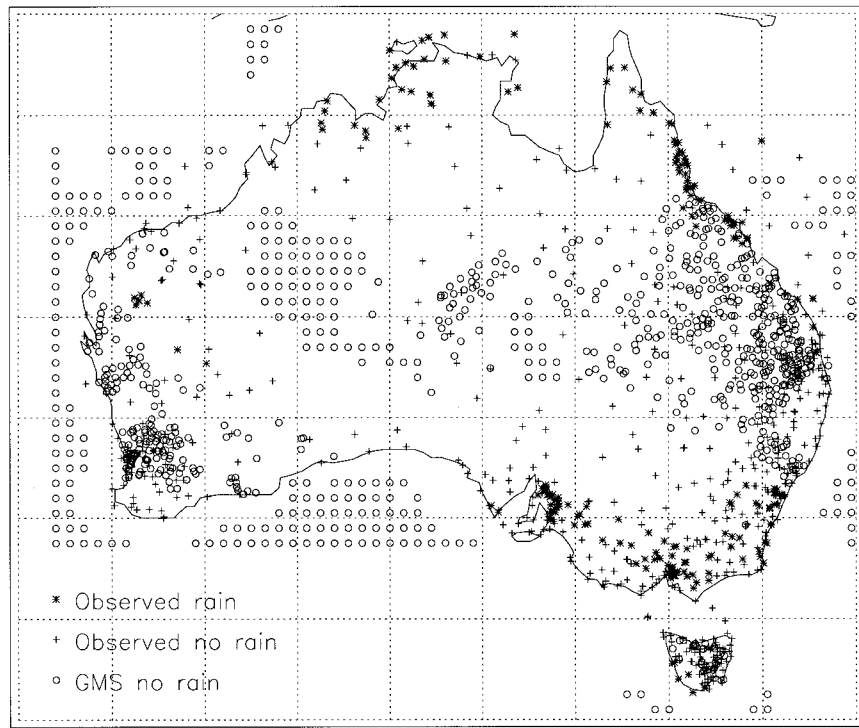


FIG. 11. Satellite no-rain observations for 24 December 1996.

a simple temperature threshold. An average accuracy of 98% in the detection of no rain can be achieved by applying a constant threshold of $\Delta T_{\min}^* = -13$ K. The average spatial coverage using this approach was 45%, which is roughly half of the observed space-time frequency of no rain. By using multiple thresholds of -30 ,

-20 , and -10 K to delineate low-, moderate-, and high-risk areas, the accuracy was maintained, while the average spatial coverage was increased to 54%.

The satellite no-rain observations were sampled so as to replace nonreports from telegraphic stations wherever possible, and at a density of one per $(75 \text{ km})^2$ in the

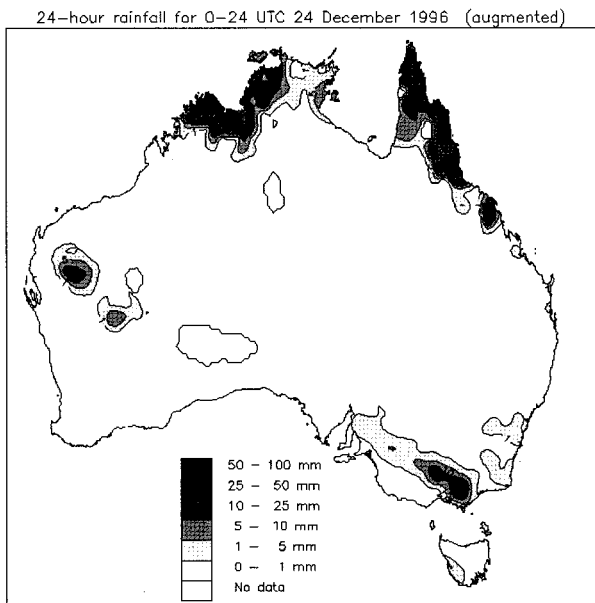


FIG. 12. Analysis of real-time rain gauge data augmented by satellite no-rain observations for 24 December 1996.

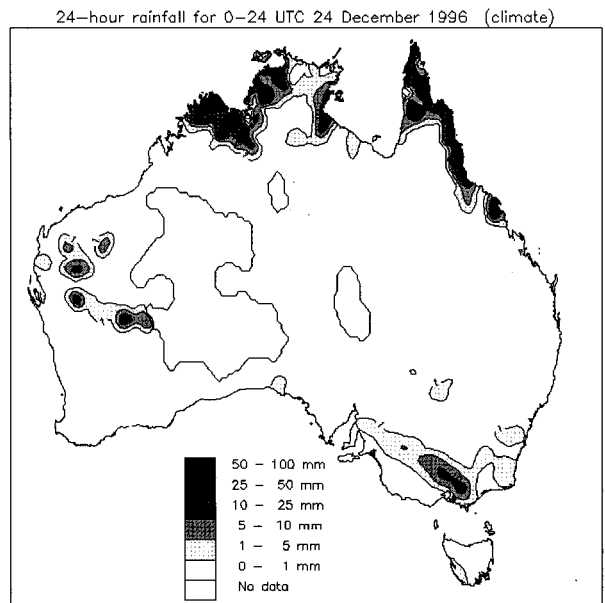


FIG. 13. Analysis of all available surface rainfall observations for 24 December 1996.

TABLE 2. Verification of rainfall analyses against independent rainfall observations from the cooperative network.

	Gauge only	Gauge + satellite
All stations (mm day ⁻¹) (528 826 samples, average rain rate = 2.02 mm day ⁻¹)		
Bias error	0.31	0.17
rms error	5.07	4.99
Mean absolute error	1.59	1.55
Raining stations (mm day ⁻¹) (107 850 samples, average rain rate = 9.90 mm day ⁻¹)		
Bias error	-0.91	-1.25
rms error	10.28	10.31
Mean absolute error	5.39	5.47
Dry stations (mm day ⁻¹) (420 976 samples, average rain rate = 0 mm day ⁻¹)		
Bias error	0.62	0.54
rms error	2.61	2.27
Mean absolute error	0.62	0.54

data-void regions. These were added to the gauge observations and analyzed to a 0.25° grid using a three-pass Barnes objective analysis scheme. When verified against independent surface rainfall observations, the satellite-augmented analyses had a substantially lower overall bias than did the gauge-only analyses with no appreciable change in rms and mean absolute errors. The most noticeable impact of the additional satellite observations was the marked reduction in the size of the data-void regions.

The addition of satellite no-rain observations increased the value of the real-time daily rainfall analyses. It could equally be applied to improve a posteriori daily

rainfall analyses that use all available surface observations; in this case only the data-void regions would be affected. The methods described in this study are applicable to other parts of the world with sparse rain gauge coverage, including many regions in Asia, Africa, and South America.

It is possible to refine the satellite rain cloud detection algorithm by including additional spectral data. Visible imagery aids in the detection of low-level and subpixel-scale cloudiness, both of which appear warm in the IR imagery. Split-window IR data can be used to detect nonprecipitating thin cirrus and eliminate these otherwise cold clouds from being detected as potential rain clouds. Infrared imagery at 3.9 μm, such as is measured from the GOES I-M geostationary satellites, provides information on the droplet size at cloud top, which is related to the probability of rain (Vicente 1996). To include these additional data would triple the processing time—whether the improvement in rain cloud detection would warrant the increased use of resources is unknown.

Another step that can be taken is to eliminate, as much as is possible, the timing differences between the GMS minimum temperature composites and the surface rainfall measurements. The use of gridded observed daily minimum temperatures, as opposed to the climatological values, in the generation of ΔT_{min} fields would improve the accuracy of the technique. These data will be used when they become operationally available.

In this study we used a Barnes successive corrections scheme to analyze the surface and satellite observations. This method was chosen because it is the scheme cur-

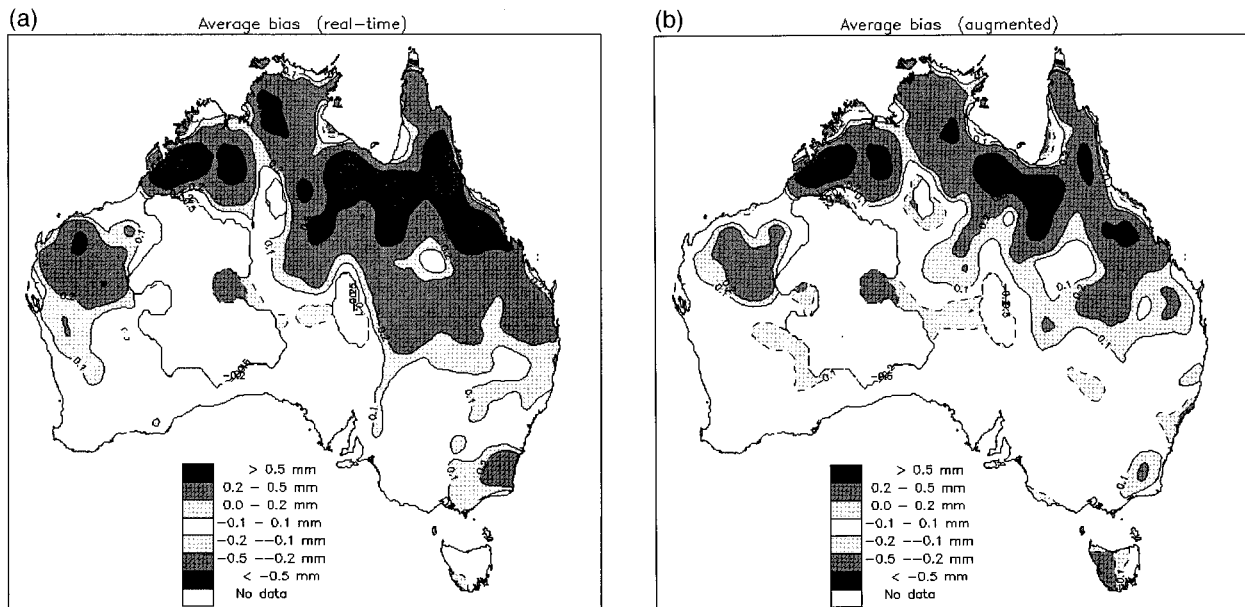


FIG. 14. Average bias relative to an analysis of all available surface rainfall observations for (a) analyses using real-time gauges only and (b) analyses of real-time rain gauge data augmented by satellite no-rain observations for the verification period 22 October 1996–23 May 1997.

rently used in the operational daily rainfall analysis scheme (Weymouth et al. 1998), but some studies suggest that other analysis schemes may be more accurate. Bussieres and Hogg (1989) found that Gandin's statistical interpolation technique produced the most accurate rainfall analyses over a network of rain gauges in Ontario, Canada. Kriging and cokriging are similar to statistical interpolation and are often used in rainfall analysis (e.g., Seo et al. 1990; Bigg 1991). The expected impact of adding satellite no-rain observations would continue to be positive, regardless of the analysis technique.

This technique can be used augmented to blend radar observations of rain–no rain with satellite surrogate no-rain observations and real-time rain gauge measurements. The addition of finer-scale radar observations would allow for much greater detail in the rainfall analysis, rendering it more useful for local hydrological applications. We anticipate incorporating radar data into future rainfall analyses.

Acknowledgments. The authors would like to thank Dr. David Jones, formerly of the Australian National Climate Centre, for providing the gridded monthly mean daily minimum surface temperature data, and Dr. Mike Manton for his helpful suggestions during the course of this work.

REFERENCES

- Achtemeier, G. L., 1987: On the concept of varying influence radii for a successive corrections objective analysis. *Mon. Wea. Rev.*, **115**, 1760–1771.
- Adler, R. F., and A. J. Negri, 1988: A satellite infrared technique to estimate tropical convective and stratiform rainfall. *J. Appl. Meteor.*, **27**, 30–38.
- Arkin, P. A., 1979: The relationship between fractional coverage of high cloud and rainfall accumulations during GATE over the B-scale array. *Mon. Wea. Rev.*, **107**, 1382–1387.
- , and B. N. Meisner, 1987: The relationship between large-scale convective rainfall and cold cloud over the Western Hemisphere during 1982–84. *Mon. Wea. Rev.*, **115**, 51–74.
- Barrett, E. C., 1970: The estimation of monthly rainfall from satellite data. *Mon. Wea. Rev.*, **98**, 322–327.
- Bigg, G. R., 1991: Kriging and intraregional rainfall variability in England. *Int. J. Climatol.*, **11**, 663–675.
- Bussieres, N., and W. Hogg, 1989: The objective analysis of daily rainfall by distance weighting schemes on a mesoscale grid. *Atmos.–Ocean*, **27**, 521–541.
- Coakley, J. A., 1988: Dynamic threshold method for obtaining cloud cover from satellite imagery data. *J. Geophys. Res.*, **92** (D4), 3985–3990.
- Drosowsky, W., 1993: An analysis of Australian seasonal rainfall anomalies: 1950–1987. Part I: Spatial patterns. *Int. J. Climatol.*, **13**, 1–30.
- Ebert, E. E., and J. Le Marshall, 1995: An evaluation of infrared satellite rainfall estimation techniques over Australia. *Aust. Meteor. Mag.*, **44**, 177–190.
- , M. J. Manton, P. A. Arkin, R. J. Allam, G. E. Holpin, and A. Gruber, 1996: Results from the GPCP Algorithm Intercomparison Programme. *Bull. Amer. Meteor. Soc.*, **77**, 2875–2887.
- Goodman, B., W. P. Menzel, E. C. Cutrim, and D. W. Martin, 1993: A non-linear algorithm for estimating 3-hourly rain rates over Amazonia from GOES/VISSR observations. *Remote Sens. Rev.*, **10**, 169–177.
- Keenan, T. D., and M. J. Manton, 1996: Darwin Climate Monitoring and Research Station: Observing precipitating systems in a monsoon environment. BMRC Research Rep. 53, 31 pp. [Available from Bureau of Meteorology, G.P.O. Box 1289K, Melbourne, Victoria, Australia 3001.]
- Negri, A. J., R. F. Adler, and P. J. Wetzel, 1984: Rain estimation from satellites: An examination of the Griffith–Woodley technique. *J. Climate Appl. Meteor.*, **23**, 102–116.
- Saunders, R. W., and K. T. Kriebel, 1988: An improved method for detecting clear sky and cloudy radiances from AVHRR data. *Int. J. Remote Sens.*, **9**, 123–150.
- Seo, D.-J., W. F. Krajewski, A. Azimi-Zonooz, and D. S. Bowles, 1990: Stochastic interpolation of rainfall data from rain gages and radar using cokriging; 2. Results. *Water Resour. Res.*, **22**, 615–622.
- Sumner, G., 1988: *Precipitation: Process and Analysis*. John Wiley and Sons, 455 pp.
- Todd, M. C., E. C. Barrett, and M. J. Beaumont, 1995: Satellite identification of rain days over the Upper Nile River basin using an optimum infrared rain/no-rain threshold temperature model. *J. Appl. Meteor.*, **34**, 2600–2611.
- UKMO/NRA, 1992: Evaluation of FRONTIERS forecast precipitation accumulation. Final Report of the Joint Met. Office-National Rivers Authority Pilot Operational Service of FRONTIERS Forecasts Assessment Group, 84 pp. [Available from UK Met Office, Bracknell, Berkshire, RG12 2SY United Kingdom.]
- Vicente, G. A., 1996: Algorithm for rainfall rate estimation using a combination of GOES-8 11.0- and 3.9-micron measurements. Preprints, *8th Conf. Satellite Meteorology and Oceanography*, Atlanta, GA, Amer. Meteor. Soc., 274–278.
- Weymouth, G., G. A. Mills, D. Jones, E. E. Ebert, and M. J. Manton, 1998: A continental-scale daily rainfall analysis system. *Aust. Meteor. Mag.*, in press.